NUMERICAL ANALYSIS OF FUEL EFFECTS ON ADVANCED COMPRESSION IGNITION USING A COOPERATIVE FUEL RESEARCH ENGINE COMPUTATIONAL FLUID DYNAMICS MODEL

Krishna Kalvakala
Department of Mechanical and Industrial Engineering, University of Illinois at Chicago, Chicago, IL 60607
Email: rkalva4@uic.edu

Pinaki Pal[1]
Energy Systems Division, Argonne National Laboratory,
9700 S Cass Avenue, Lemont, IL 60439
Email: pal@anl.gov

Yunchao Wu
Department of Mechanical Engineering, University of Connecticut,
Storrs, CT 06269
Email: yunchao.wu@uconn.edu

Goutham Kukkadapu
Lawrence Livermore National Laboratory,
Livermore, CA 94550
Email: kukkadapu1@llnl.gov

Christopher Kolodziej
Energy Systems Division, Argonne National Laboratory,
9700 S Cass Avenue, Lemont, IL 60439
Email: ckolodziej@anl.gov

Jorge Pulpeiro Gonzalez
Energy Systems Division, Argonne National Laboratory,
9700 S Cass Avenue, Lemont, IL 60439
Email: jpulpeirogonzalez@anl.gov

Muhammad Umer Waqas
Energy Systems Division, Argonne National Laboratory,
9700 S Cass Avenue, Lemont, IL 60439
Email: mwaqas@anl.gov

[1]Corresponding author.

Tianfeng Lu
Department of Mechanical Engineering, University of Connecticut,
Storrs, CT 06269
Email: tianfeng.lu@uconn.edu

Suresh K. Aggarwal
Department of Mechanical and Industrial Engineering, University of Illinois at Chicago,
Chicago, IL 60607
Email: ska@uic.edu

Sibendu Som
Energy Systems Division, Argonne National Laboratory,
9700 S Cass Avenue, Lemont, IL 60439
Email: ssom@anl.gov

ABSTRACT

Growing environmental concerns and demand for better fuel economy are driving forces that motivate the research for more advanced engines. Multi-mode combustion strategies have gained attention for their potential to provide high thermal efficiency and low emissions for light-duty applications. These strategies target optimizing the engine performance by correlating different combustion modes to load operating conditions. The extension from boosted SI mode at high loads to advanced compression ignition (ACI) mode at low loads can be achieved by increasing compression ratio and utilizing intake air heating. Further, in order to enable an accurate control of intake charge condition for ACI mode and rapid mode-switches, it is essential to gain fundamental insights into the autoignition process. Within the scope of ACI, homogeneous charge compression ignition (HCCI) mode is of significant interest. It is known for its potential benefits, operation at low fuel consumption, low NOx and PM emissions. In the present work, a virtual Cooperative Fuel Research (CFR) engine model is used to analyze fuel effects on ACI combustion. In particular, the effect of fuel Octane Sensitivity (S) (at constant RON) on autoignition propensity is assessed under beyond-RON (BRON) and beyond-MON (BMON) ACI conditions. The 3D CFR engine computational fluid dynamics (CFD) model employs finite-rate chemistry approach with multi-zone binning strategy to capture autoignition. Two binary blends with Research Octane Number (RON) of 90 are chosen for this study: Primary reference fuel (PRF) with S = 0, and toluene-heptane (TH) blend with S = 10.8, representing paraffinic and aromatic gasoline surrogates. Reduced mechanisms for these

blends are generated from a detailed gasoline surrogate kinetic mechanism. Simulation results with the reduced mechanisms are validated against experimental data from an in-house CFR engine, with respect to in-cylinder pressure, heat release rate and combustion phasing. Thereafter, the sensitivity of combustion behavior to ACI operating condition (BRON vs BMON), air-fuel ratio (λ = 2 and 3), and engine speed (600 and 900rpm) is analyzed for both fuels. It is shown that the sensitivity of a fuel's autoignition characteristics to λ and engine speed significantly differs at BRON and BMON conditions. Moreover, this sensitivity is found to vary among fuels, despite the same RON. It is also observed that the presence of low temperature heat release (LTHR) under BRON condition leads to more sequential autoignition and longer combustion duration than BMON condition. Finally, the study indicates that the octane index (OI) fails to capture the trend in the variation of autoignition propensity with S under BMON condition.

Keywords: Computational fluid dynamics, Homogeneous Charge Compression Ignition, CFR engine, Low temperature heat release, Thermal stratification

INTRODUCTION

Currently, transportation sector is predominantly powered by hydrocarbon-based fuels. It is predicted that they will continue to contribute a significant share (~70%) to power transportation across the world even in 2050 [1]. On the flip side, the transportation sector accounted for nearly 40% of total CO_2 emissions in 2019, and certainly with the increase in demand for mobility, this share is estimated to increase in the near future. This stands as the prime motivation for continuous research in identifying

new combustion strategies and develop engines with improved efficiency and lower emissions.

Two representative modes of operation in engines are spark ignition (SI) and compression ignition (CI). SI engines are characterized by flame propagation and with small modifications can achieve low tailpipe soot and NO_x emissions, but they are compromised to operate at lower efficiencies due to limitations associated with cyclic variability and knocking [2,3]. CI engines operate at relatively higher compression ratios, which make them more fuel efficient at all load conditions. However, conventional CI diesel engines suffer from relatively high tailpipe emissions of nitric oxides (NO_x) and particulate matter (PM). In this context, an efficient way to optimize engine performance and lower emissions is to implement multi-mode strategies. These strategies target optimizing the engine performance by correlating different combustion modes to load operating conditions. This allows to capitalize on advantages from different (existing or new) combustion modes of operation. Thus, within the scope of light duty vehicles, multi-mode combustion strategies have gained attention for their ability to provide high thermal efficiency and low emissions. A potential multi-mode strategy would entail mode-switching from boosted SI at high loads to an advanced compression ignition (ACI) mode at low loads. Several ACI modes are under consideration, while the interest lies in engines operating in the low temperature combustion (LTC) regime. LTC is a very promising technology that has attracted significant interest in recent developments of internal combustion engines. It is known for its potential to achieve high efficiencies along with ultra-low NO_x and soot emissions. The main idea is to deploy highly diluted, nearly

homogeneous fuel-air mixtures by using combustion products and other means [4]. Homogenous charge compression ignition (HCCI), Premixed Charged Compression Ignition (PCCI), and Reactivity Controlled Compression Ignition (RCCI) are some of the known variants of this strategy [5-9]. Among these ACI strategies, HCCI is the most preliminary mode explored and has gained significant interest as this mode of operation can itself be considered a combination of SI and CI engine modes. Fuel and air are premixed like SI engines, however the mixture is leaner in HCCI mode, while it is compressed to allow autoignite like CI engines. This means, the combustion phenomena and associated heat release are mainly governed by autoignition characteristics of the fuel. In other words, the HCCI mode of operation is mainly governed by chemical kinetics of the fuel, which is known to depend on the fuel chemical composition, in addition to operating conditions like engine speed, intake pressure (P_{in}) and intake temperature (T_{in}) of the fuel/air mixture. Even though this mode has potential benefits like low emissions and high thermal efficiency, there are limitations associated with control over autoignition of such lean fuel/air mixtures. Thus, in order to fit in HCCI mode of operation within the scope of a multi-mode strategy, it is essential to gain fundamental insights into the auto-ignition process. These insights will feed in to control the intake charge condition for ACI operation and hence, to achieve smooth, rapid mode-switches in a multi-mode engine configuration.

HCCI-like conditions have been of interest for several decades. Some potential parameters and phenomena that impact autoignition are thermal stratification, fuel/mixture stratification, fuel composition and associated fuel properties [10-24]. In

order to better understand the effects of addition of biofuels and associated changes in fuel properties on autoignition performance, Calam et al. [7] investigated the impact of mixing different alternative fuels, such as ethanol, methanol, fusel oil, butanol and iso-propanol, with n-heptane on combustion performance under HCCI engine conditions. Combustion performance was observed to be strongly related to fuel properties – heat of vaporization, evaporation temperature and octane number. However, it must be noted that each of these properties is strongly dependent on the fuel composition. Yao et al. [15] in an experimental study tested different fuels, including gasoline, PRF and mixtures of PRF and ethanol, at different operating conditions. It was observed that in addition to fuel composition effects, the combustion characteristics of a fuel also significantly depend on the operating condition. Moreover, it was found that autoignition, and HC and CO emissions have good correlation with the octane index (OI) at all conditions, and for all fuel blends other than the one with ethanol. Kalghatgi [2] introduced OI, defined as:

$$\mathrm{OI} = \mathrm{RON} - \mathrm{K} * (\mathrm{RON} - \mathrm{MON}) \tag{1}$$

where RON and MON are the Research Octane Number and Motor Octane Number, respectively, while *K* is an empirical constant representative of the pressure-temperature (P-T) history of the unburnt mixture. Further, studies [25-27] have shown that a change in fuel chemical composition has a significant effect on low temperature (LTHR) and intermediate temperature (ITHR) heat release, which subsequently impact the main stage heat release or autoignition characteristics. It was observed that presence of LTHR allows for stable combustion, and extension of HCCI operation to higher load limits. In addition, Sjöberg et al. [27] showed that LTHR is highly dependent on engine speed. For instance,

for PRF80 fuel, the LTHR decreased by a factor 15 or nearly vanished when engine speed increased from 1050 to 1500rpm. In a more recent study, Waqas et al. [28] observed through a series of experiments that for a given fuel, the LTHR phenomena primarily depend on the intake valve closing (IVC) conditions, implying that LTHR varies significantly with operating conditions (T_{in} and P_{in}). In addition, two other factors that have prominent impact on autoignition characteristics are thermal and fuel stratification. Thermal stratification to some extent is naturally induced by wall heat transfer and turbulent convection. This allows the mixture to autoignite sequentially from the hottest regions to the coldest, thereby resulting in lower heat release rates and longer combustion duration. Several studies [10, 29-35] have characterized the significance of thermal stratification using experimental and computational (0-D and CFD) techniques. It was observed that thermal stratification has a more dominant effect when compared to fuel stratification [10, 33]. Further, it was shown that thermal stratification can be artificially enhanced by inducing higher turbulent intensity [31], by using negative valve overlap (NVO) [10, 32, 33], and through direct injection of water in the form of thermally stratified compression ignition (TSCI) concept [30]. On the other hand, several studies also highlighted the effect of fuel stratification on combustion control in HCCI engines [36-38]. Fuel stratification becomes effective for fuels which show high ϕ-sensitivity, a fuel characteristic defined based on the relationship between ignition delay timing and equivalence ratio [36]. Tao et al. [37] and Pintor et al. [38] have investigated the effect of equivalence ratio on ignition delay under representative P-T trajectories for various gasoline like fuels. It was observed that fuels having high ITHR and those exhibiting negative temperature coefficient (NTC)

behavior show strong ϕ-sensitivities, while fuels that have no NTC behavior displayed small or zero ϕ-sensitivity. Studies have also shown that fuel octane sensitivity (*S*) depends on NTC behavior [13,39,40,41]. Fuel propensity to exhibit ITHR and/or NTC behavior significantly depends on the IVC pressure and temperature conditions [37, 38]. Both higher intake pressures and low temperatures tend to increase ITHR and thus, increase the ϕ-sensitivity.

Based on the above discussion, it is well understood that the autoignition behavior of a fuel under HCCI mode has a complex dependency on fuel composition, properties and engine operating conditions. Therefore, in order to extend the applicability of HCCI to multi-mode strategies, it is of paramount importance to explore the properties/conditions that optimize fuel-engine interaction. The Co-Optimization of Fuels and Engines, or the "Co-Optima" initiative of the US Department of Energy [42] aims to explore pathways to enable such synergistic development of advanced fuels and engines for higher efficiency and lower emissions. Within the context of Co-Optima initiative, the central fuel property hypothesis (CFPH) states that for a given engine platform, fuel properties are sufficient to characterize the performance of the engine, irrespective of the fuel chemical composition. Recently, Szybist et al. [43] and Pal et al. [44] have explored this hypothesis for boosted SI conditions, through experiments and CFD simulations, respectively. Several fuel blends of interest to Co-Optima were investigated, and the results showed that OI was a reasonably good indicator of knock propensity. Overall, they found that the fuels generally behaved in accordance with CFPH, except that some fuels consistently outperformed (or underperformed) the OI expectations. Further,

in the context of HCCI engines, there is also continuous interest in understanding the performance of OI in LTC engines for various operating conditions [45, 46]. Pintor and Dec et al. [45] have explored this hypothesis experimentally and investigated gasoline-like fuels for four P-T trajectories, which include beyond-MON (BMON), MON, RON and beyond-RON (BRON) HCCI conditions. It was observed that equivalence ratio and speed had a significant impact on the capability of OI to characterize autoignition propensity. The OI performed reasonably well for all operating conditions, other than BRON. However, reasons for the same were not investigated.

The objective of the present numerical work is to provide insights related to fuel effects on autoignition propensity under HCCI combustion mode. Two binary fuel mixtures with constant RON of 90, but different *S*, are examined under BRON and BMON conditions. As a first step, the numerical setup is validated against experimental data for PRF and TH fuels under BRON and BMON conditions. Thereafter, the validated numerical setup is used to characterize combustion behavior under two global equivalence ratios (ϕ = 0.3 and 0.5) and at two engine speeds (600 and 900rpm). In addition, the effects of thermal stratification on ignition and rate of heat release are also analyzed.

EXPERIMENTAL AND MODELING SETUPS

1. CFR Engine Platform

The experimental results shown in this work are based on the tests performed on an in-house CFR F1/F2 engine at Argonne National Laboratory (ANL). This is a carbureted single-cylinder engine which is used to measure a fuel's RON and MON based on ASTM protocols [47, 48]. In order to make it suitable for HCCI mode of operation, the standard

knockmeter was replaced by a Kistler 6045-AU20 pressure transducer, which allowed to acquire cylinder pressure data. In addition, the standard carburetor horizontal jet was made smaller to achieve lean (near air-fuel ratio (lambda, λ) of 3) premixed HCCI operation. An absolute measurement of air-fuel ratio was obtained by adding a wide-band lambda sensor in the standard ASTM exhaust line between the port and exhaust surge tank. Flush mounted high-speed pressure transducers were used to obtain intake and exhaust port pressures with crank-angle resolution. Cycle-averaged intake and exhaust temperatures were obtained with K-type thermocouples. The local crank angle resolved in-cylinder pressure data was triggered using a crankshaft encoder with resolution of 0.1 crank angle degrees. Table 1 shows some of the key specifications of this engine, while more details are discussed elsewhere [28, 49].

2. Fuels and Operating Conditions

The autoignition characteristics of two binary blends, PRF and TH (toluene/n-heptane), are studied in this work. RON of both fuels is the same (= 90), while S values are 0 and 10.8, respectively. Table 2 shows the composition (in terms of mass fraction) of the fuel blends.

For each fuel blend, experimental data is obtained for λ = 3 and engine speed = 600rpm, under both BRON (P_{in} = 1.3bar, T_{in} = 52^0C) and BMON (P_{in} = 1.0bar, T_{in} = 149^0C) conditions. Figure 1 shows a comparison of the P-T trajectories (during compression) of the two operating conditions with those of the standard CFR RON and MON 90 tests [40]. 300 pressure cycles were recorded for each test condition. The compression ratio is adjusted to ensure that CA50 (crank angle of 50% fuel mass fraction burned) is fixed at ~3

CAD (±1 CAD) ATDC for all operating conditions under consideration. This dataset is utilized for CFD model validation. Subsequently, for the numerical study, a broader test matrix is considered, as shown in Table 3, to investigate effects of lambda and engine speed.

3. Numerical Model

A virtual CFR engine model developed at ANL has been extensively employed in previous studies to study SI engine combustion characteristics [44, 50, 51, 52]. This model, with minor modifications, is used in the present study to investigate HCCI mode of operation. The key modification adopted in the engine geometry is the removal of the spark plug.

Figure 2 shows the computational domain representing the engine geometry. A commercial 3D CFD code CONVERGE (version 2.3) [53], is used to perform full-cycle engine simulations. The grid generation in computational domain is performed by COVERGE during runtime, with the capability of increasing the grid resolution via fixed embedding and adaptive mesh refinement (AMR). Fixed embedding enables the use of high grid resolution in regions of interest *a priori*, while AMR refines the grid during runtime based on gradients of temperature and velocity. In this study, a base grid of 2mm is used outside the cylinder, while 1mm base grid is used inside the cylinder. Two levels of fixed embedding (cell size of 0.5mm) is adopted near the cylinder head, piston and liner. Additionally, AMR of two levels is employed based on sub-grid criterion of 1 m/s and 2.5 K for velocity and temperature, respectively [54, 55]. This results in a peak cell count of around 1.3 million cells. The in-cylinder turbulence is modeled using unsteady

RANS based re-normalized group (RNG) k-ε model [56] with wall functions. The wall heat transfer is accounted for by using the Han and Reitz model [57]. A second-order central differencing scheme is used for spatial discretization and a first-order implicit scheme is employed for temporal discretization. The time step is controlled using the diffusive and convective Courant-Friedrichs-Lewy (CFL) numbers with a maximum value of 1.0 between IVC and EVO. Realistic intake/exhaust boundary conditions were prescribed based on experiments. Wall temperatures were estimated by a 1D GT-Power model.

In-cylinder combustion is modeled using finite-rate chemistry approach combined with the multi-zone strategy. The Co-Optima gasoline detailed kinetic model developed by Mehl et al. [58], containing nearly 2300 chemical species and 10,000 chemical reactions, is used to generate skeletal mechanisms for each fuel blend; reduction techniques based on directed relation graph (DRG), DRG-aided sensitivity analysis (DRGASA), isomer lumping are employed [59-62]. The resulting skeletal mechanisms for PRF and TH blends contain 178 and 181 species, respectively. These mechanisms are validated against a wide range of experimental data available for homogenous ignition delay timing as well as CFR engine data as discussed in the Model Validation section.

4. Numerical Methodology

The homogeneous ignition delay calculations presented in this paper are based on simulations of homogeneous fuel-air mixtures under constant volume conditions, performed using CHEMKIN-Pro [63]. The state of first-stage ignition delay (FIDT) is defined as the interval from the initial time to the instant of first peak in temperature rise rate. The total or main stage ignition delay (MIDT) is defined as the time interval from initial

point to the time instant when the mixture temperature increases by 400K over one computational time step [4,13,14].

Each CFD simulation is run using 80 processors on the Blues computing cluster at ANL. Approximate run time for each engine cycle is around 40 hours. Six consecutive cycles are simulated for each fuel and for every operating condition. However, the first two cycles were neglected to remove any effect of initial conditions. Thus, all observations made in this paper are based on results for cycles 3-6. Moreover, in order to remain consistent with CFR engine experiments, the CA50 for each fuel, at every condition is fixed at ~3 CAD (±1 CAD) by adjusting the compression ratio (CR).

The operating condition is referenced as '#fuelname-#condition-#L-#Speed'. For instance, PRF-BRON-L3-600rpm indicates that the fuel is PRF, P-T trajectory is BRON (boosted condition), λ = 3, and engine speed is 600rpm. In addition, throughout the discussion, the two terms λ and ϕ are used interchangeably. Physically both indicate the degree of fuel-air premixing, and they are related as $\lambda = \frac{1}{\phi}$.

MODEL VALIDATION

The skeletal mechanisms developed for PRF and TH have been validated against different types of experimental data. Figure 3 presents a comparison between shock-tube ignition delay measurements for PRF91 [64] and TH [65] blends with the respective numerical results obtained from simulations performed using CHEMKIN-Pro. Overall, there is a good agreement between the measurements and predictions from the skeletal mechanisms. Figure 4 presents a comparison of experimental in-cylinder pressure and

heat release rate (HRR) profiles with those obtained from CFD simulations for BRON-L3-600rpm condition. Figure 5 presents the corresponding results for BMON-L3-600rpm condition. The experimental pressure trace shown is an average of 300 consecutive cycles, while the CFD results are based on cycle 4. We noticed negligible cycle-to-cycle variation in CFD, and hence only results of one cycle (cycle 4 here) are presented. Once again, the CFD simulations capture the evolution of in-cylinder pressure and HRR reasonably well for both fuels. Also, the trends in low temperature heat release (LTHR) under BRON conditions are well captured. In addition, the compression ratios required in experiments and simulations to achieve a CA50 of ~3.0 CAD ATDC are very similar, with the values for simulations lower than those in experiments. Under BRON-L3-600rpm conditions, experimental compression ratios for PRF and TH blends are 12.84 and 13.62, while those used in simulations are 11.5 and 12.2, respectively. Similarly, under BMON-L3-600rpm conditions, experimental compression ratios for PRF and TH blends are 14.05 and 13.33, while for CFD simulations these are 11.92 and 11.42, respectively. Hence, the trends in compression ratio are well captured by the simulations.

RESULTS AND DISCUSSION

To elucidate the importance of *S* and OI in characterizing the autoignition propensity of gasoline-like fuels under different P-T trajectories, this section is broadly divided into four sub-sections. The first sub-section addresses the importance of fuel composition and associated LTHR on autoignition characteristics by comparing the PRF and TH blends under BRON and BMON conditions. Further, the subsequent sub-sections discuss the

effects of thermal stratification, equivalence ratio and engine speed, respectively, on the fuel autoignition behavior.

1. Effects of Fuel Composition

Figures 4 and 5 depict the in-cylinder pressure traces and HRR profiles for PRF and TH blends, under BRON-L3-600rpm and BMON-L3-600rpm conditions, respectively. It is evident that under BRON conditions, both the fuels show significant amount of LTHR. However, there are differences in terms of the start and amount of LTHR. The reason for these differences can be explained by comparing the P-T trajectories and first-stage ignition delay contours (Fig. 6a). Figure 6 shows the first-stage and main-stage ignition delay iso-contours for PRF and TH fuels at ϕ = 0.3 and 600rpm operating conditions. In addition, a comparison of P-T trajectories from engine simulations at ϕ = 0.3 are shown for both BRON and BMON conditions. It can be noticed that the first-stage ignition delay retards with increase in *S*, which indicates earlier timing of LTHR occurrence under BRON conditions for the fuel with smaller *S*. This is consistent with the CFD results where the start of LTHR occurs earlier (by ~1.2 CAD) for PRF (*S* = 0) when compared to TH blend (*S* = 10.8), where the start of LTHR is defined by a criterion of 0.2 J/CAD [28]. On the other hand, due to high temperatures and low pressures associated with BMON condition, the P-T trajectories tend to avoid the low temperature regime or the region that exhibits prominent LTHR. Therefore, there is no evidence of LTHR for both fuels under BMON conditions in CFD. These observations are also consistent with results published in recent studies [28, 37].

Further, under both BRON and BMON conditions, CFD results suggest that CA10 (crank angle at 10% mass burned), which is used as an indication of autoignition in CI engines, occurs earlier for the PRF. In particular, CA10 for PRF occurs earlier than TH fuel by ~1.85 CAD and ~0.85 CAD, under BRON-L3-600rpm and BMON-L3-600rpm conditions, respectively. The higher reactivity of PRF can be justified with the help of main-stage ignition delay calculations. Figure 6b presents a comparison of MIDT iso-contours for both fuels along with the P-T trajectories for BRON-L3-600rpm and BMON-L3-600rpm conditions. Large differences in MIDT can be observed between the two fuels at intermediate pressures (20-40bar) and intermediate temperatures (700-900K). This is a typical NTC region for any fuel. PRF has significantly higher MIDT than TH blend in these regions. However, the trend reverses under high temperatures (>920K) where PRF has lower MIDT values. This suggests that PRF is more reactive than TH fuel in the high temperature regions (>920K), irrespective of pressure. Further, this is the region of autoignition based on CFD simulations (as seen from P-T trajectories) for both BRON and BMON conditions. Thus, the observation from CFD that PRF is more reactive or has advanced CA10 than TH blend, is consistent with the analysis of P-T trajectories and MIDT iso-contours.

Lastly, the difference in CA10s of PRF and TH blends decreases when transitioning from BRON (~1.85 CAD) to BMON (~0.85 CAD) conditions. This change in behavior is predominantly a consequence of LTHR. To elaborate, higher amount of LTHR for PRF-BRON-L3-600rpm condition also results in higher fraction of mass consumed between start and end of LTHR. The fraction of mass consumed during LTHR in PRF and TH blends

is ~4.9% and 3.6%, respectively. In addition, as discussed earlier, PRF is more reactive than TH blend under high temperature regions. Both these effects add up resulting in the overall advancement in CA10 of PRF relative to TH blend under BRON condition. However, LTHR is not present under BMON conditions. Thus, the difference in CA10 observed under BMON conditions is only a consequence of MIDT differences. Hence, the CA10s for PRF and TH blends are much closer under BMON conditions.

Based on previous studies [2, 43, 45], it is evident that the value of *K* in OI definition (Eq. 1) is < 0 for BRON conditions, and > 0 for BMON conditions. In terms of autoignition quality of a fuel, this indicates that the fuel with higher *S* is more resistant to autoignition under BRON conditions, while the same fuel tends to ignite much earlier (less resistant) under BMON conditions. However, based on the CA10 results from CFD, the fuel with higher *S* is more resistant to autoignition under both BRON and BMON conditions. Thus, it violates OI prediction under BMON conditions. This indicates that fuel response is highly dependent on the ACI strategy being used.

2. Significance of Thermal Stratification

The analysis of thermal stratification and its impact on autoignition phenomenon is also carried out. Figure 7 illustrates the temporal evolution of thermal stratification in terms of coefficient of variance (CoV) up to CA10 for PRF90 under BRON and BMON L3-600rpm conditions. CoV is defined based on Eqs. (2) and (3), where T_i is the local temperature in the cylinder at a grid cell and *n* is the total number of grid points in the cylinder. In general, CoV can be interpreted as relative variability of the data around the

mean. Higher value of CoV indicates greater level of dispersion around the mean. In other words, higher CoV for temperature indicates greater thermal stratification in the cylinder.

$$CoV = \frac{Standard\ Deviation\ (T_{std})}{Mean\ (\overline{T})} \times 100 \quad (2)$$

$$T_{std} = \left(\frac{\sum_{i=1}^{n}(T_i - \bar{T})^2}{n-1}\right)^{1/2} \quad (3)$$

As seen in Fig. 7, thermal stratification to some degree is observed under both BRON and BMON conditions. However, it is significantly higher under BRON conditions. The increase in CoV under BRON conditions is associated with the occurrence of LTHR (as seen in Fig. 4). The higher thermal stratification results in longer CA10–CA50 under BRON condition (5.66 CAD) compared to BMON conditions (2.8 CAD). This is characteristic of enhanced sequential autoignition, suggesting that heat release rate during ACI operation under BRON conditions may be more controllable (via LTHR) than operation under BMON conditions.

3. Effects of Equivalence Ratio

Figure 8 shows the autoignition sensitivity of PRF and TH blends (in terms of ΔCA10) to changes in equivalence ratio (ϕ = 0.3 and 0.5, at 600rpm) under BRON and BMON conditions. ΔCA10 associated with change in ϕ is greater for PRF. Also, ΔCA10 becomes less significant when transitioning from BRON to BMON conditions, irrespective of the chosen fuel. This suggests that the fuel with higher octane sensitivity (*S*) is less sensitive to varying ϕ, and BRON conditions are more susceptible to equivalence ratio variations.

To better understand the behavior of fuels under different P-T trajectories, an attempt is made to relate the CFD results with that of 0-D ignition delay calculations. Figure 9 shows the first-stage and main-stage ignition delay iso-contours for PRF at ϕ = 0.3 and 0.5. In addition, a comparison of P-T trajectories at ϕ = 0.3 and 0.5 is also shown for both BRON and BMON conditions. It can be clearly seen that FIDT is nearly insensitive to change in ϕ, while the MIDT considerably decreases for richer mixtures. However, the differences in MIDT are higher under low temperatures and the NTC regimes. Consequently, it is expected that a larger variation of chemical reactivity and fuel ignition performance will be observed for BRON conditions compared to BMON conditions. The TH blend also shows similar behavior (not shown here for the sake of brevity). Therefore, this analysis based on 0-D simulations is consistent with that observed from CFD simulations, which indicates that the fuels are more ϕ-sensitive under BRON conditions as evident from higher ΔCA10s.

4. Effects of Engine Speed

In this section, the effect of increasing engine speed from 600 to 900 rpm on autoignition characteristics under BRON and BMON-L3 conditions is discussed. The critical CR required to achieve a CA50 of ~3.0 CAD ATDC increases with engine speed. Figure 10 shows a comparison of critical compression ratios (CRs) for PRF and TH blends under different operating conditions. For instance, the critical CRs required at 600rpm and 900rpm engine speeds are 11.5 and 13.49, respectively, or ΔCR=1.99, for PRF under BRON conditions. On the other hand, the ΔCR for PRF under BMON condition is 1.2. Evidently, ΔCR reduces when transitioning from BRON to BMON conditions. This is due to the fact

that the lower residence time at higher engine speed suppresses LTHR (as shown in Fig. 11). Hence, the BRON conditions which show more LTHR than BMON conditions, exhibit a larger ΔCR with engine speed. This reasoning also explains the observation from Fig. 10 that the difference in critical CR between the two blends decreases with engine speed, irrespective of the operating condition.

CONCLUSIONS

In the scope of multi-mode strategies, a computational study was carried out to evaluate fuel effects under ACI (HCCI) conditions using the virtual CFR engine model. Two blends, PRF and TH, having same RON (=90) and octane sensitivities (*S*) of 0 and 10.8, respectively were chosen. Skeletal reaction mechanisms for these blends were developed from a detailed mechanism and were validated against experimental data. Effect of varying operating conditions (BRON versus BMON relevant conditions), ϕ (0.3 versus 0.5), and engine speed (600rpm versus 900rpm) were investigated. It was observed that occurrence of LTHR has a significant impact on the overall combustion behavior. The presence of LTHR increased the thermal stratification, which resulted in a more stable or controlled combustion process in the cylinder. While the LTHR was quite evident under BRON conditions, there was no evidence of its occurrence under BMON conditions. The higher amount of LTHR under all BRON P-T trajectories, helped to achieve desirable longer combustion phasing when compared to BMON P-T trajectories. Further, the significance of LTHR under BRON increased with increase in ϕ (0.3 to 0.5), while it reduced at higher engine speeds due to lower residence time available under low temperature regimes. Both the fuels were more ϕ-sensitive under BRON conditions. It was also shown that the

octane index (OI) fails to capture the trend in the variation of autoignition propensity with *S* under BMON conditions.

ACKNOWLEDGMENTS

The submitted manuscript has been created by UChicago Argonne, LLC, Operator of Argonne National Laboratory (Argonne). Argonne, a U.S. Department of Energy (DOE) Office of Science laboratory, is operated under Contract No. DEAC02-06CH11357. The U.S. Government retains for itself, and others acting on its behalf, a paid-up nonexclusive, irrevocable worldwide license in said article to reproduce, prepare derivative works, distribute copies to the public, and perform publicly and display publicly, by or on behalf of the Government. This research was partially funded by DOE's Office of Vehicle Technologies and Office of Energy Efficiency and Renewable Energy under Contract No. DE-AC02-06CH11357. The authors wish to thank Gurpreet Singh, Kevin Stork, and Michael Weismiller, program managers at DOE, for their support. This research was conducted as part of the Co-Optimization of Fuels & Engines (Co-Optima) project sponsored by the U.S. Department of Energy (DOE) Office of Energy Efficiency and Renewable Energy (EERE), Bioenergy Technologies and Vehicle Technologies Offices.

The authors would like to acknowledge the computing facilities, the Laboratory Computing Resource Center (LCRC) at Argonne National Laboratory and University of Illinois at Chicago, for computing time used in this research.

REFERENCES

[1]https://www.eia.gov/outlooks/aeo/pdf/AEO2020%20Full%20Report.pdf

[2] Kalghatgi, G.T., 2013, “Fuel/Engine Interactions”, SAE International, Warrendale, PA.

[3] Chen C., Pal P., Ameen M., Feng D., Wei H., 2020, “Large-eddy simulation study on cycle-to-cycle variation of knocking combustion in a spark ignition engine”, Applied Energy, Vol. 261 (1), 114447.

[4] Kukkadapu G., Kumar K., Sung C.J., Mehl M., and Pitz W.J., 2015, “Autoignition of gasoline surrogates at low temperature combustion conditions.” Combust. Flame. Vol. 162 (5) pp. 2272-2285.

[5] Epping K., Aceves S., Bechtold R., and Dec J.E., 2002, “The potential of HCCI combustion for high efficiency and low emissions.” SAE Technical Paper 2002–01-1923.

[6] Chang J., Kalghatgi G., Amer A., and Viollet Y., 2012, “Enabling high efficiency direct injection engine with naphtha fuel through partially premixed charge compression ignition combustion.” SAE Technical Paper; 2012–01-0677.

[7] Calam A., Aydogan B., and Halis S., 2020, “The comparison of combustion, engine performance and emission characteristics of ethanol, methanol, fusel oil, butanol, isopropanol and naphtha with n-heptane blends on HCCI engine”, Fuel Vol. 226, 117071.

[8] Sun C., Kang D., Bohac S.V., and Boehman A.L., 2016, “Impact of fuel and injection timing on partially premixed charge compression ignition combustion.” Energy Fuels, Vol. 30, pp. 4331-4345.

[9] Reitz R.D., Duraisamy G., 2015, “Review of high efficiency and clean reactivity-controlled compression ignition (RCCI) combustion in internal combustion engines.” Prog. Combut. Sci. Vol. 46, pp: 12-71.

[10] Kodavasal J., Lavoie G.A., Assanis D.N., and Martz J.B., 2015, “The effects of thermal and compositional stratification on the ignition and duration of homogeneous charge compression ignition combustion”, Combust. Flame, Vol. 162, pp: 451-461.

[11]Sjöberg M., and Dec J.E., 2007, “Comparing late cycle autoignition stability for single and two stage ignition fuels in HCCI engines”, Proc. Combust. Inst. Vol. 31 (2), pp: 2895-2902.

[12] Kim S., Kim J., Shah A., Pal P., Scarcelli R., Rockstroh T., Som S., Wu Y., and Lu T., 2019, “Numerical study of advanced compression ignition and combustion in a gasoline direct injection engine”, Proceedings of the ASME 2019 ICEF Division Fall technical conference, ICEF2019-7281: V001T06A013, doi: 10.1115/ICEF2019-7281.

[13] Jain S.K., and Aggarwal S.K., 2018, “Compositional effects on the ignition and combustion of low octane fuels under diesel conditions”, Fuel Vol. 220, pp: 654-670.

[14] Fu X., Aggarwal S.K., 2015, “Two stage ignition and NTC phenomenon in diesel engines”, Fuel, Vol. 144, pp. 188-196.

[15] Liu H., Yao M., Zhang B., and Zheng Z., 2009, “Influence of fuel and operating conditions on combustion characteristic of a homogeneous charge compression ignition”, Energy Fuel Vol. 23(3), pp: 1422-30.

[16] Cui Y., Liu H., Geng C., Tang Q., Feng L., Wang Y., Yi W., Zheng Z., and Yao M., 2020, “Optical diagnostics on the effects of fuel properties and coolant temperatures on combustion characteristic and flame development progress from HCCI to CDC via PPC”, Fuel Vol. 269, 117441.

[17] Pal P., Keum S.H., Im H.G., 2015, “Assessment of flamelet versus multizone combustion modeling approaches for stratified-charge compression ignition engines.” Int. J. Engine Research, Vol. 17 (3), pp. 280-290.

[18] Keum S.H., Pal P., Im H.G., Babajimopoulos A., and Assanis D.N., 2015, “Effects of fuel injection parameters on the performance of homogeneous charge compression ignition at low-load conditions.” Int. J. Engine Research, Vol. 17 (4), pp. 413-420.

[19] Fu X., and Aggarwal S.K., 2015, “Fuel unsaturation effects on NOx and PAH formation in spray flames” Fuel, Vol. 160, pp. 1-15.

[20] Pal P., Valorano M., Arias P.G., Im H.G., Woolridge M.S., Ciottoli P.P., and Galassi R.M., 2017, “Computational characterization of ignition regimes in a syngas/air mixture with temperature fluctuations”, Proc. Combust. Inst., Vol. 36 (3), pp. 3705-3716.

[21] Im H.G., Pal P., Wooldrige M.S. and Mansfield A.B., 2015, “A regime diagram for autoignition of homogeneous reactant mixtures with turbulent velocity and temperature fluctuations.” Combust. Sci. Tech., Vol. 187 (8), pp. 1263-1275.

[22] Pal, P., Mansfield, A.B., Wooldridge, M.S., Im, H.G., 2015, “Characteristics of Syngas Auto-ignition at High Pressure and Low Temperature Conditions with Thermal Inhomogeneities”, Energy Procedia, Vol. 66, pp. 1-4.

[23] Pal P., Mansfield A.B., Arias P.G., Wooldrige M.S., and Im H.G., 2015, “A computational study of syngas auto-ignition characteristics at high-pressure and low-temperature conditions with thermal inhomogeneities.” Combust. Theory Modelling Vol. 19 (5), pp. 587-601.

[24] Pal P., 2016, “Computational modelling and analysis of low temperature combustion regimes for advanced engine applications.” Ph.D. dissertation, University of Michigan, Ann Arbor, MI.

[25] Shibata G., Oyama K., Urushihara T., and Nakano T., 2004, “The effect of fuel properties on low and high temperature heat release and resulting performance of an HCCI engine”, SAE Technical Paper 2004-01-0553.

[26] Lu X., Hou Y., Zu L., Huang Z., 2006, “Experimental study on the autoignition and combustion characteristics in the homogeneous charge compression ignition (HCCI) combustion operation with ethanol/n-heptane blend fuels by port injection”, Fuel Vol. 85 (17-18), pp: 2622-31.

[27] Sjöberg M., and Dec J.E., 2007, “EGR and intake boost for managing HCCI low temperature heat release over wide ranges of engine speed”, SAE Technical Paper 2007-01-0051.

[28] Waqas M.U., Hoth A., Kolodziej C.P., Rockstroh T., Pulpeiro Gonzalez J., and Johansson B., 2019, “Detection of low temperature heat release (LTHR) in the standard cooperative fuel research (CFR) engine in both SI and HCCI combustion modes”, Fuel Vol. 256, pp:115745.

[29] Lawler B., Mamalis S., Joshi S., Lacey J., Guralp O., Najt P., and Filipi Z., 2017, “Understanding the effect of operating conditions on thermal stratification and heat release in a homogeneous charge compression ignition engine”, Applied thermal engineering Vo. 112, pp: 392-402.

[30] Lawler B., Splitter D., Szybist J., and Kaul B., 2017, “Thermally stratified compression ignition: A new advanced low temperature combustion mode with load flexibility”, Applied Energy Vol. 189, pp: 122-132.

[31] Yu R., Bai X.S., Lehtiniemi H., Ahmed S.S., Mauss F., Ritcher M., Alden M., Hildingsson L., Johansson B., and Hultqvist A., 2006, “Effect of turbulence and initial temperature inhomogeneity on homogeneous charge compression ignition engine”, SAE Technical Paper 2006-01-3318.

[32] Joelsson T., Yu R., Sjoholm J., Tunestal P., and Bai X.S., 2010, “Effects of negative valve overlap on the auto-igntion process of lean ethanol/air mixture in HCCI engines”, SAE Technical Paper 2010-01-2235.

[33] Sofianopoulos A., Boldaji M.R., Lawler B., and Mamalis S., 2018, “Analysis of thermal stratification effects in HCCI engines using large eddy simulations and detailed chemical kinetics”, SAE Technical Paper 2018-01-0189.

[34] Dronniou N., and Dec J.E., 2012, “Investigating the development of thermal stratification from near wall regions to the bulk gas in an HCCI engine with planar imaging thermometry”, SAE Int. J. Eng. Vol. 5(2012-01-1111), pp: 1046-1074.

[35] Snyder J., Dronniou N., Dec J., and Hanson R., 2011, “PLIF measurements of thermal stratification in an HCCI engine under fired operation.” SAE Int. J. Eng. Vol. 4, pp: 1669-1688 (2011-01-1291).

[36] Yang Y., Dec J., Dronniou N., Sjöberg M., and Cannella W., 2011, “Partial fuel stratification to control HCCI heat release rates: Fuel composition and other factors affecting pre-ignition reactions of two staged ignition fuels”, SAE Int. J. Engines Vol. (4) (1), pp.1903-1920.

[37] Tao M., Zhao P., Szybist J.P., Lynch P., and Ge H., 2019, “Insights into engine autoignition: Combining engine thermodynamic trajectory and fuel ignition delay iso-contour”, Combust. Flame Vol. 200, pp: 207-218.

[38] Pintor D.L., Dec J., and Gentz G., 2019, “ϕ-sensitivity for LTGC engines: understanding the fundamentals and tailoring fuel blends to maximize this property”, SAE Technical Paper 2019-01-0961.

[39] Kalghatgi G., Babiker H., and Badra J., 2015, “A simple method to predict knock using toluene, n-heptane and iso-octane blends (TPRF) as gasoline surrogates.” SAE Int. J. Engines Vol. 8, pp: 505-519.

[40] Singh E., Badra J., Mehl M., and Sarathy S.M., 2017, “Chemical kinetics insights into the octane number and octane sensitivity of gasoline surrogate mixtures”, Energy Fuels Vol. 31(2), pp: 1945-60.

[41] Leppard, W.R., 1990, “The chemical origin of fuel octane sensitivity”, Journal of Fuels and Lubricants, pp. 862-876.

[42] https://www.energy.gov/eere/bioenergy/co-optimization fuels-engines

[43] Szybist S., and Splitter D., 2018, “Understanding chemistry-specific fuel differences at a constant RON in a boosted SI engine”, Fuel, Vol. 217, pp. 370-381.

[44] Pal P., Kalvakala K., Wu Y., McNenly M., Lapointe S., Whitesides R., Lu T., Aggarwal S.K., and Som S., 2020, “Numerical investigation of a central fuel property hypothesis under boosted spark ignition conditions”, *J. Energy Resour. Technol.,* Vol. 143(3) 032305 (8 pages).

[45] Pintor D. L., and Dec J., 2020, “Understanding the performance of OI in LTGC engines from beyond MON to beyond RON”, Advanced Engine Combustion Review Meeting.

[46] Pintor D. L., Dec J., and Gentz G., 2020, “Experimental evaluation of a custom gasoline like blend designed to simultaneously improve phi-sensitivity, RON and octane sensitivity”, SAE Technical Paper 2020-01-1136.

[47]ASTM D2699-12, 2012, “Standard test method for Research Octane Number of spark ignition engine fuel.” ASTM International, West Conshohocken, PA.

[48] ASTM D2700-16, 2016, “Standard test method for Motor Octane Number of spark ignition engine fuel.” ASTM International, West Conshohocken, PA.

[49] Hoth A., Gonzalez P.J., Kolodziej C., and Rockstroh T., 2019, “Effects of Lambda on knocking characteristics and RON rating”, SAE Int. J. Adv. & Curr. Prac. in Mobility Vol. 1(3), pp:1188-1201.

[50] Pal P., Kolodziej C., Choi S., Som S., Broatch A., Sariano J.G., Wu Y., Lu T., and See Y.C., 2018, “Development of a virtual CFR engine model for knocking combustion analysis” SAE Int. J. Engines, Vol. 11 (6), pp. 1069-1082.

[51] Pal P., Wu Y., Lu T., Som S., See Y.C., and Le Moine A., 2018, “Multidimensional numerical simulations of knocking combustion in a cooperative fuel research engine”, *J. Energy Resour. Technol.,* Vol 140 (10), 102205 (8 pages)

[52] Pal P., Wu Y., Lu T., Som S., See Y.C., and Le Moine A., 2017, “Multi-dimensional CFD simulations of knocking combustion in a CFR engine”, Proceedings of the ASME 2019 ICEF Division Fall technical conference, ICEF2019-7284: V002T06A017, doi:10.1115/ICEF2019-7284.

[53] CONVERGE 2.3 Theory Manual, Convergent Science Inc., Middleton, WI, 2016.

[54] Pal, P., Probst, D., Pei, Y., Zhang, Y.,Traver M., Cleary D., Som S., 2017, “Numerical Investigation of a Gasoline-Like Fuel in a Heavy-Duty Compression Ignition Engine Using Global Sensitivity Analysis,” *SAE Int. J. Fuels Lubr.* Vol. 10(1), pp. 56-68.

[55] Pei, Y., Pal, P., Zhang, Y., Traver, M., Cleary D., Futterer C., Brenner M., Probst D., and Som S., 2019, “CFD-guided combustion system optimization of a gasoline range fuel in a heavy-duty compression ignition engine using automatic piston geometry generation and a supercomputer”, *SAE Int. J. Adv. & Curr. Prac. in Mobility* Vol. 1(1) pp. 166-179.

[56] Han Z., and Reitz R.D., 1995, “Turbulence Modeling of Internal Combustion Engines Using RNG k-ε Models”, Combust. Sci. Technol, Vol. 106, pp: 267-295, doi: 10.1080/00102209508907782.

[57] Han Z., and Reitz R.D., 1997, “A Temperature Wall Function Formulation for Variable Density Turbulence Flow with Application to Engine Convective Heat Transfer Modeling,” Int. J. Heat Mass Transfer. Vol. 40(3) pp: 613-625, doi: 10.1016/0017-9310(96)00117-2.

[58] Mehl M., Zhang Z., Wagnon S., Kukkadapu G., Westbrook C.K., Pitz W., Zhang Y., Curran H., Al. Rachidi M., and Sarathy M.S., 2018, “A comprehensive detailed kinetic mechanism for the simulation of transportation fuels”, 10th US National Combut. Meeting, pp.1-6.

[59] Lu, T., Law, C.K., 2005, “A Directed Relation Graph Method for Mechanism Reduction”, Proc. Combust. Inst, Vol. 30(1), pp. 1333-1341.

[60] Zheng, X.L., Lu, T., Law, C.K., 2007, “Experimental Counterflow Ignition Temperatures and Reaction Mechanisms of 1,3-butadiene”, Proc. Combust. Inst, Vol. 31(1), pp. 367-375.

[61] Lu, T., Law, C.K., 2008, “Strategies for Mechanism Reduction for Large Hydrocarbons: n-heptane”, Combust. Flame, Vol. 154(1), pp. 153-163.

[62] Wu, Y., Pal, P., Som, S., Lu, T., 2017, “A skeletal Chemical Kinetic Mechanism for Gasoline and Gasoline/Ethanol Blend Surrogates for Engine CFD Applications”, International Conference on Chemical Kinetics.

[63] CHEMKIN-PRO 15141, Reaction Design, San Diego, 2015

[64] AlAbbad M., Javed T., Khaled F., Badra J., and Farooq A., 2017, “Ignition delay time measurements of primary reference fuel blends”, Combust. Flame Vol. 178, pp: 205-216.

[65] Herzler J., Fikri M., Hitzbleck K., Starke R., Schulz C., Roth P., Kalghatgi G.T., 2007, “Shock-tube study of the autoignition of n-heptane/toluene air mixtures at intermediate temperatures and high pressures”, Combust. Flame Vol. 149, pp: 25-31.

Figure Captions List

Fig. 1 P-T trajectories of the BRON and BMON (at λ = 3 and 600rpm) conditions considered in this study, along with standard CFR RON and MON 90 tests.

Fig. 2 Computational domain of the virtual CFR engine.

Fig. 3 Validation of skeletal mechanisms against homogeneous ignition delay time measurements for (a) PRF91 [64] and (b) TH blends [65]. Symbols denote experimental data and lines denote computational results.

Fig. 4 Comparison of experiments (solid lines) and CFD simulations (dashed lines) in terms of in-cylinder pressure trace and heat release rate profiles for PRF (blue) and TH (red) under BRON-L3-600rpm condition.

Fig. 5 Comparison of experiments (solid lines) and CFD simulations (dashed lines) in terms of in-cylinder pressure trace and heat release rate profiles for PRF (blue) and TH (red) under BMON-L3-600rpm condition.

Fig. 6 Numerical in-cylinder thermodynamic (P-T) trajectories for BRON-L3 and BMON-L3 overlapped on the iso-contours of (a) first-stage ignition delay and (b) main-stage ignition delay for PRF and TH blends.

Fig. 7 Temporal evolution of temperature stratification for PRF up to CA10 under BRON and BMON conditions at L3-600rpm.

Fig. 8 ΔCA10 due to differences in ϕ (0.3 to 0.5 at 600rpm) for PRF (S = 0) and TH (S = 10.8) fuels.

Fig. 9 Numerical in-cylinder thermodynamic (P-T) trajectories of BRON-L3-600rpm and BRON-L2-600rpm overlapped on the iso-contours of (a) first-stage ignition delay and (b) main-stage ignition delay for PRF.

Fig. 10 Comparison of critical compression ratios for constant CA50 of ~3.0 CAD ATDC at different operating conditions.

Fig. 11 Comparison of heat release profiles of PRF under BRON-L3-600 and BMON-L3-900 conditions.

Table Caption List

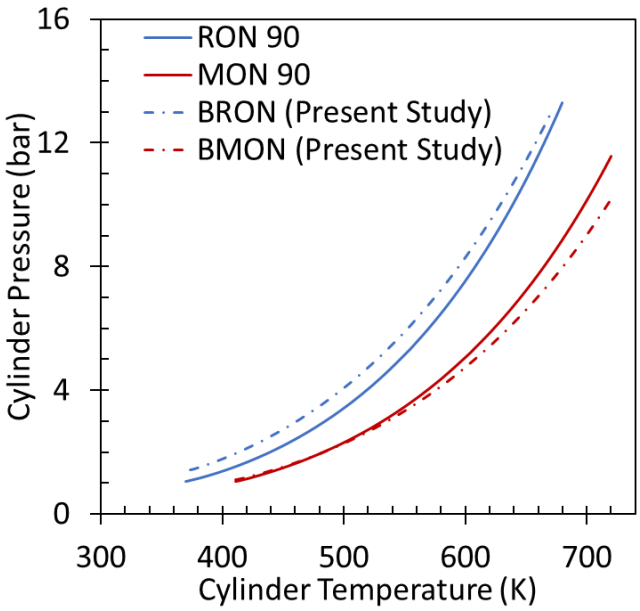

Figure 1. P-T trajectories of the BRON and BMON (at λ = 3 and 600rpm) conditions considered in this study, along with standard CFR RON and MON 90 tests.

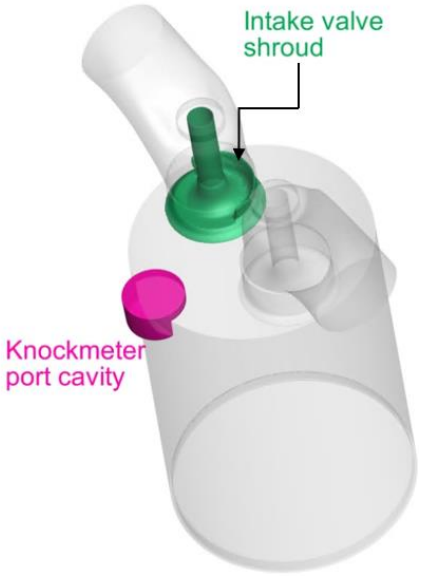

Figure 2. Computational domain of the virtual CFR engine.

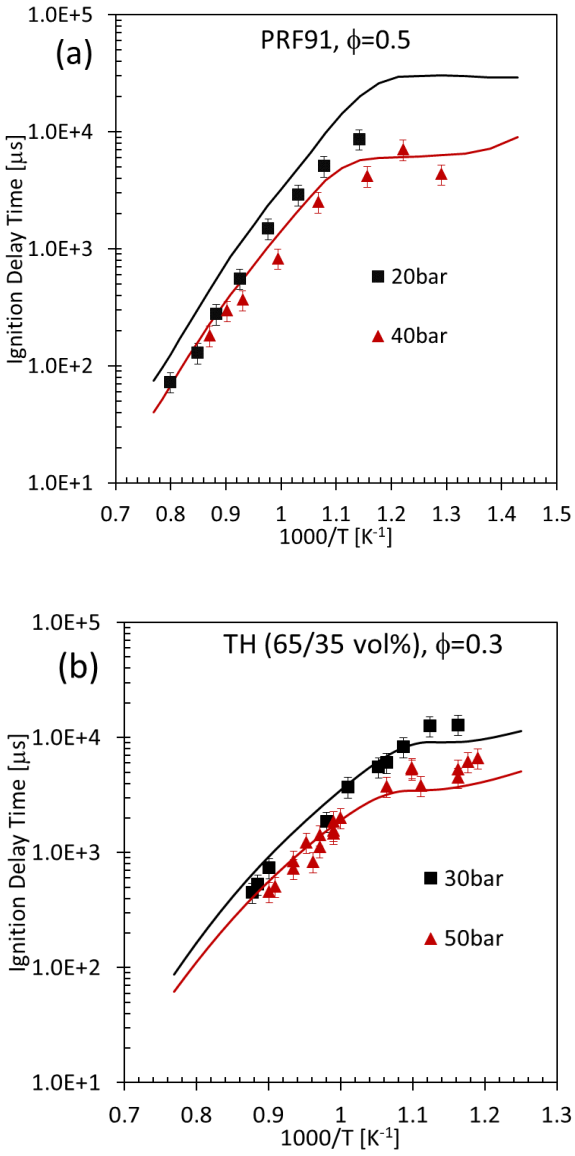

Figure 3. Validation of skeletal mechanisms against homogeneous ignition delay time measurements for (a) PRF91 [64] and (b) TH [65] blends. Symbols denote experimental data and lines denote computational results.

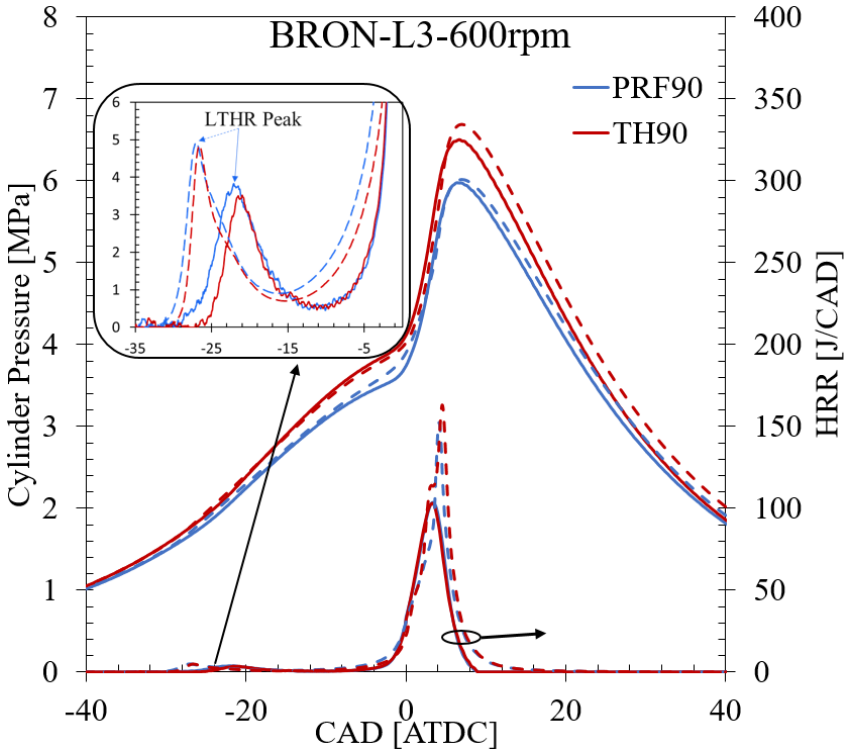

Figure 4. Comparison of experiments (solid lines) and CFD simulations (dashed lines) in terms of in-cylinder pressure trace and heat release rate profiles for PRF (blue) and TH (red) under BRON-L3-600rpm condition.

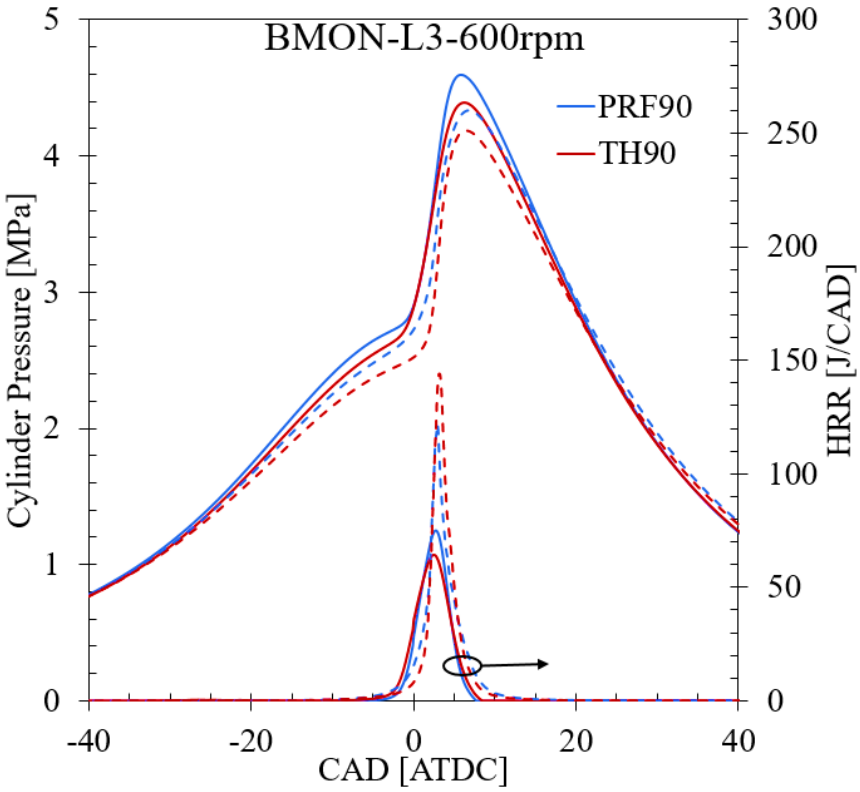

Figure 5. Comparison of experiments (solid lines) and CFD simulations (dashed lines) in terms of in-cylinder pressure trace and heat release rate profiles for PRF (blue) and TH (red) under BMON-L3-600rpm condition.

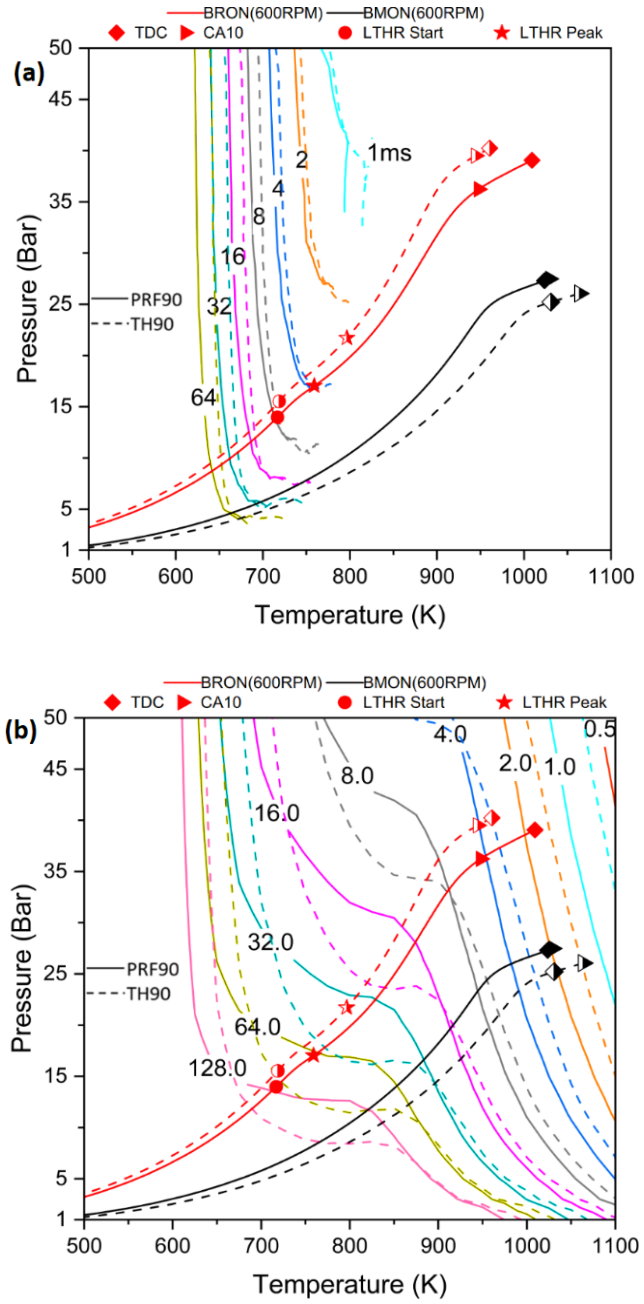

Figure 6. Numerical in-cylinder thermodynamic (P-T) trajectories for BRON-L3 and BMON-L3 overlapped on the iso-contours of (a) first-stage ignition delay and (b) main-stage ignition delay for PRF and TH blends.

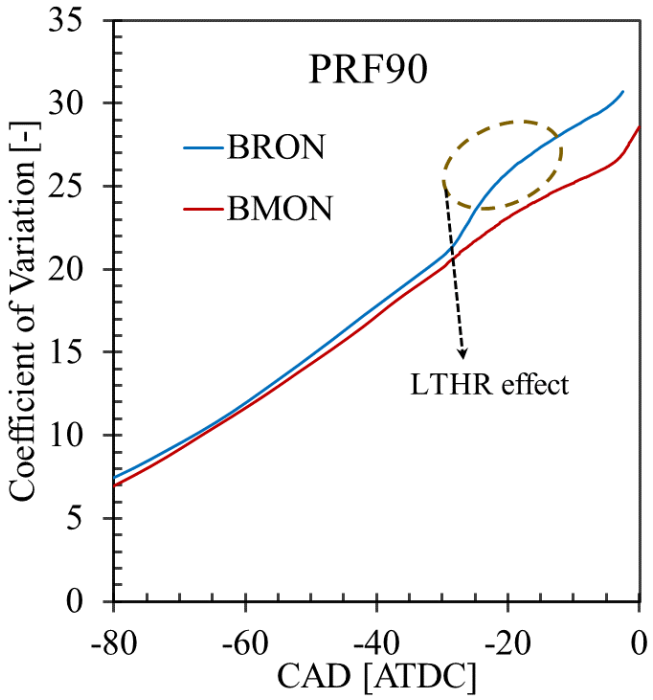

Figure 7. Temporal evolution of temperature stratification for PRF up to CA10 under BRON and BMON conditions at L3-600rpm.

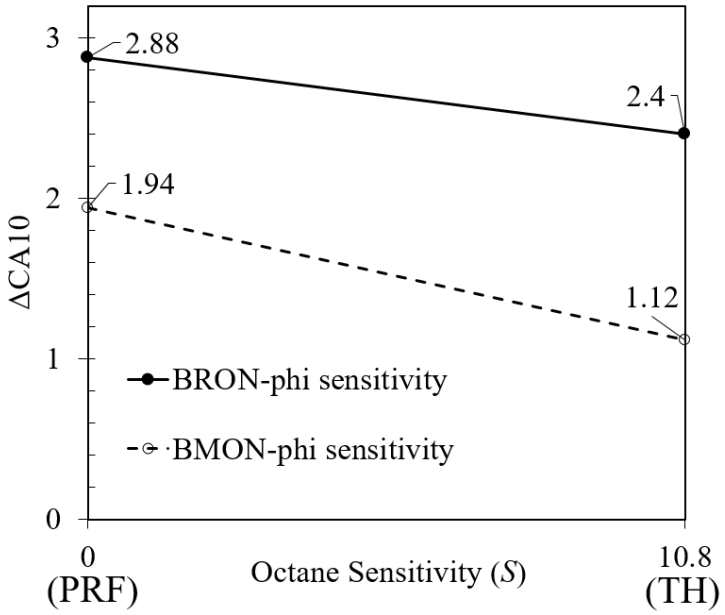

Figure 8. ΔCA10 due to differences in ϕ (0.3 to 0.5 at 600rpm) for PRF (*S* = 0) and TH (*S* = 10.8) fuels.

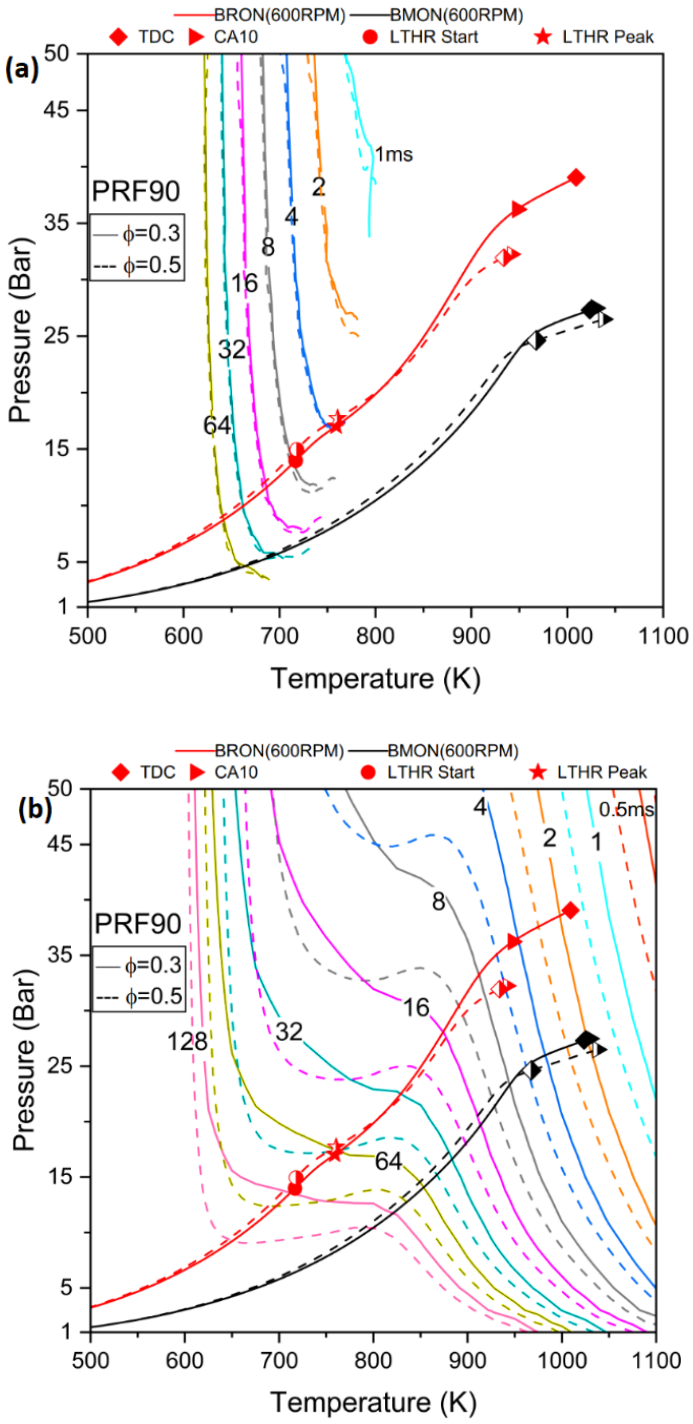

Figure 9. Numerical in-cylinder thermodynamic (P-T) trajectories of BRON-L3-600rpm and BRON-L2-600rpm overlapped on the iso-contours of (a) first-stage ignition delay and (b) main-stage ignition delay for PRF.

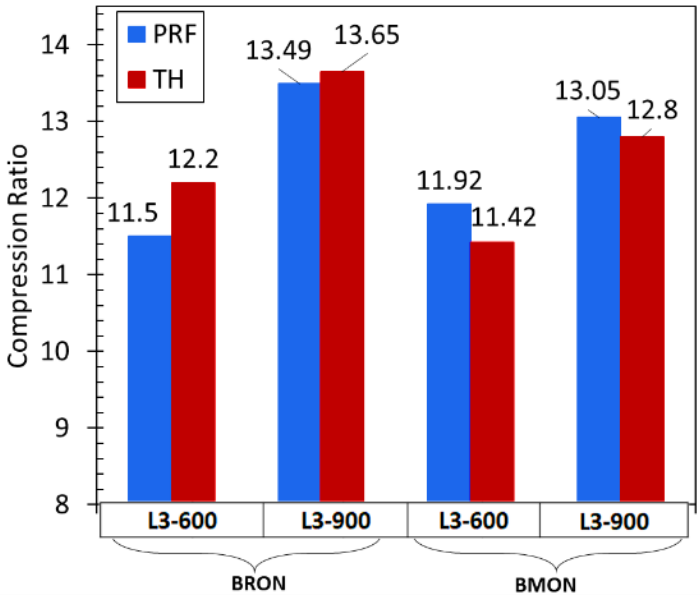

Figure 10. Comparison of critical compression ratios for constant CA50 of ~3.0 CAD ATDC at different operating conditions.

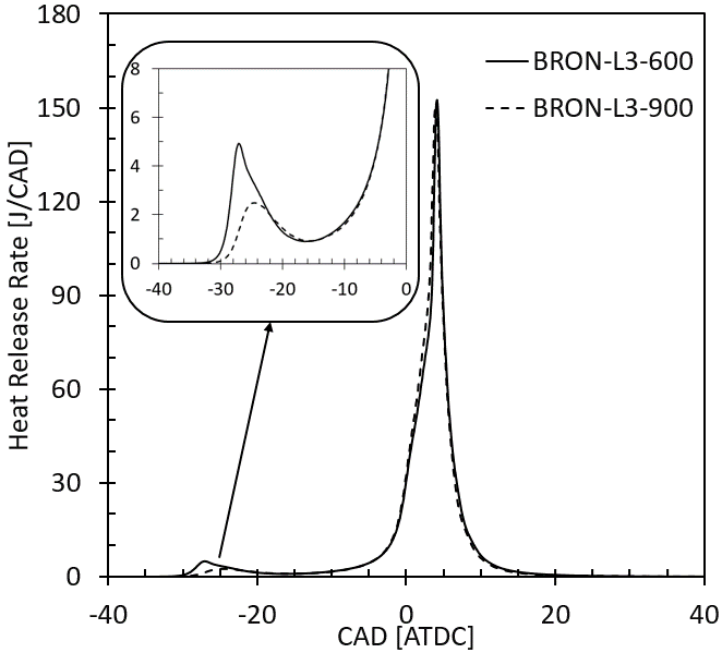

Figure 11. Comparison of heat release profiles of PRF under BRON-L3-600 and BMON-L3-900 conditions.

Table 1: *CFR Engine Specifications*

Stroke/Bore (mm)	114.3/82.55
Connecting Rod (mm)	254
Intake Valve Open (IVO)	10^0 ATDC
Intake Valve Close (IVC)	34^0 ABDC
Exhaust Valve Open (EVO)	40^0 BBDC
Exhaust Valve Close (EVC)	15^0 ATDC

Table 2: *Composition of the Fuel Surrogates*

	PRF	**TH**
Iso-Octane (mass fraction)	0.9	0
n-Heptane (mass fraction)	0.1	0.249
Toluene (mass fraction)	0	0.751

Table 3: *Operating Conditions for the Numerical Study*

	Intake Pressure (bar)	**Intake Temperature (^{0}C)**	λ	**Speed (rpm)**
BRON	1.3	52	3.0, 2.0	600, 900
BMON	1.0	149	3.0, 2.0	600, 900